

# Enhanced Photo-Catalytic Degradation of RhB Dyes under UV/Visible Irradiation using Sm Doped ZnFe<sub>2</sub>O<sub>4</sub> with g-C<sub>3</sub>N<sub>4</sub> Nanocomposites

Sania Arif <sup>1,\*</sup>, Hafeez Anwar<sup>1</sup>, Muhammad Sajid<sup>1</sup>, Fakhar Abbas<sup>2</sup>, Rabia Khalid<sup>1</sup>, Seerat Sadia<sup>3</sup> and Rubab Fatima<sup>4</sup>

<sup>1</sup>Department of Physics, University of Agriculture, Faisalabad-38000, Pakistan

<sup>2</sup>Department of Physics, University of the Punjab, Lahore-05422, Pakistan

<sup>3</sup>Department of Nursing, Sharif Medical College, Lahore-05422, Pakistan

<sup>4</sup>Department of Angiography, Chaudhary Pervaiz Elahi Institute of Cardiology, Wazirabad, Pakistan

\*Corresponding author: [saniaarif626@yahoo.com](mailto:saniaarif626@yahoo.com)

## Abstract

Industrial dye pollution poses a threat to ecosystems, but semiconductor photocatalysis offers a sustainable solution. In this study, Sm doped ZnFe<sub>2</sub>O<sub>4</sub> with g-C<sub>3</sub>N<sub>4</sub> composites were produced with co-precipitation for the environmental degradation of RhB dye. The composites were characterized using different methods. The synthesised samples' crystal structure was clearly visible through X-ray diffraction, with an average crystallite size of 20–30 nm and a cubic structure. The basic composition of the materials, as determined by EDX, indicates that the composite was prepared correctly. The micrographs of SEM indicate average grain sizes of 10 nm for SGZ1, 14 nm for SGZ2, and 23.14 nm for SGZ3 nanocomposites. FT-IR measurements in the 4000-400 cm<sup>-1</sup> range showed the O-H, C-N, and C=N functional groups are present. Analysis of UV-Vis spectrums showed the optical band gap value from 1.24 to 1.41eV. The ideal conditions for photocatalytic At a pH of 8, degradation was seen, and the dosage of the photocatalyst of 60mg/50mL, and an dosage of H<sub>2</sub>O<sub>2</sub> 10 mM, used a SZG3 composite. In these conditions, efficient RhB dye degradation was accomplished at 98.3% using this SZG3 composite within 70 min. Over five cycles, the reusability of the nanocomposite was also assessed.

Keywords: Co-precipitation, Composite, Heterogeneous photocatalysis, Wastewater treatment

Cite this Article as: Arif S, Anwar H, Sajid M, Abbas F, Khalid R, Sadia S, Fatima R, 2025. Enhanced photo-catalytic degradation of RhB dyes under UV/visible irradiation using Sm doped ZnFe<sub>2</sub>O<sub>4</sub> with g-C<sub>3</sub>N<sub>4</sub> nanocomposites. In: Nisa ZU, Altaf S, Zahra A and Saeed K (eds), Nanobiotech in Holistic Health: Innovations for Integrated Well-being. Unique Scientific Publishers, Faisalabad, Pakistan, pp: 97-103. <https://doi.org/10.47278/book.HH/2025.106>



A Publication of  
Unique Scientific  
Publishers

Chapter No:  
25-015

Received: 31-Jan-2025  
Revised: 07-March-2025  
Accepted: 18-May-2025

## Introduction

The textile industry's massive expansion has caused a notable rise in water contamination, primarily because of the release of industrial wastes like various inorganic and organic dyes into water sources. According to Konstantinou and Albanis, between 1 and 20% of the globally produced dyes are disappearing during the dyeing process and end up in textile effluents. The waste products from the dyeing process in these industries are highly toxic, impacting the metabolism of living organisms. They also present serious risks to human health, the environment, and natural processes such as eutrophication. The textile industry, which mainly uses synthetic dyes, is one of the major sources of these persistent organic compounds (Ebrahimi et al., 2021). Many of these dyes are dangerous to humanity and aquatic life because they are not biodegradable (Bera et al., 2018). Therefore, it is essential to break down non-biocompatible organic compounds and purify the water to preserve the ecosystem (Faheem et al., 2022). The RhB is recognised as among the most toxic dyes found in textile wastewater. It holds significant value in the textile industry as a colourant due to its exceptional stability and non-biodegradability. When RhB is used extensively, it can be toxic to the thyroid, eyes, and skin. It can also be harmful to the throat and liver (Mousavi et al., 2024). In this present work, the focus is on the degradation of RhB. Conventional wastewater treatment techniques like sedimentation, coagulation, chemical flocculation, ozonation, filtration, and so on are used in removing dyes from textile effluent (Abdulhamid & Muzamil, 2023). But these methods have a number of drawbacks, including energy consumption and toxic by-products.

Among them, photocatalysis has generated a great deal of interest because of the expense effectiveness, high efficiency, and simplicity of use. Since the 1970s, hydroxyl radicals have been used an efficient technique in oxidation processes purifying water, to reduce organic pollutants that are not biodegradable. In photocatalysis, reusable photocatalysis, along with an active source of light like sunlight and an oxidising agent like air or oxygen, are employed to degradation the organic pollutants such as dyes. Particle size reduction in this process increases the quantity of active sites and their surface area, which improves reactivity. With an increase in the number of active sites, the adsorption of pollutants on surface of the catalyst also increases (Mamba & Mishra, 2016). During the previous 20 years, research has focused on using semiconductors as photocatalysts.

Among various semiconductors, ZnFe<sub>2</sub>O<sub>4</sub> is considered particularly important due to their ability to remove organic dye contaminants, thanks to their physical and chemical properties, environmental friendliness, and stability (Shahraki et al., 2023). However, their

photocatalytic activity is only activated by UV-visible irradiation. Rare earth elements are also used in photocatalysis process due to their unique electronic properties, which boost the performance of photocatalytic materials (Rabiee et al., 2021).

The polymeric without metal photocatalyst graphite carbon nitride ( $g\text{-C}_3\text{N}_4$ ) has drawn more interest because of its non-toxicity, appropriate electron band gap (about 2.7 eV), and consistent stability. But the restricted absorption of visible light and the quick efficiency of photogenerated electron-hole pair complexation greatly limit the applications of  $g\text{-C}_3\text{N}_4$  (Rawal et al., 2013).

For the first time in this process,  $g\text{-C}_3\text{N}_4$  heterojunction with Sm-doped  $\text{ZnFe}_2\text{O}_4$  according to reports, as a supported electron mediator. In this work, a photocatalyst Sm-doped  $\text{ZnFe}_2\text{O}_4$  with different amounts of  $g\text{-C}_3\text{N}_4$  (2%, 3%, and 4%) was created and utilised to break down rhodamine B (RhB) dye in the presence of regular sunlight. The analysis of prepared material using FTIR, XRD, UV-Vis spectroscopy SEM/EDX, was used to define the functional group, crystalline structure, morphology, optical characteristics, chemical composition and purity of the created samples. The results indicate that Sm-supported  $\text{ZnFe}_2\text{O}_4$  with  $g\text{-C}_3\text{N}_4$  increases surface area and that photo-induced charge carrier separation significantly improves the photocatalyst's response to visible light.

## Experimental Work

### Synthesis of $g\text{-C}_3\text{N}_4$

The process of to create  $g\text{-C}_3\text{N}_4$ , thermal polymerisation was employed. After adding ten grams of melamine to the crucible, it was heated to 550 °C for three hours. The melamine was burned out in the furnace to produce the yellow-colored  $g\text{-C}_3\text{N}_4$  (Fu et al., 2018).

### Synthesis of Dy- $\text{ZnFe}_2\text{O}_4$

A stoichiometric ratio of  $\text{Zn}_{1-x}\text{Sm}_x\text{Fe}_2\text{O}_4$ ,  $x = 0.03$ , was used to dissolve nickel nitrate ( $\text{NO}_3)_2 \cdot 6\text{H}_2\text{O}$ , Samarium nitrate ( $\text{SM}(\text{NO}_3)_2 \cdot 6\text{H}_2\text{O}$ ), and ferric nitrate ( $\text{Fe}(\text{NO}_3)_3 \cdot 9\text{H}_2\text{O}$ ) in 50 ml of distilled water. Throughout the process of synthesis, solutions were constantly stirred to attain homogeneity, and drops of the precipitating agent (NaOH) were added to reach and maintain pH 8. After that, the solution was elevated to 80 °C for one hour. The brown color precipitate that formed due to these processes was centrifuged two times, initially with double-distilled water and then with ethanol, to eliminate the impurities and nitrate ions. After being dried for 12 hours at 70 °C, the resultant byproduct was examined. The final product was converting into tiny nanoparticles using a mortar, and the muffle furnace was used to calcine the powder at 500 °C for three hours. Several characterization techniques were used to analyze the properties of prepared material (Ullah, 2023).

### Synthesis of Sm- $\text{ZnFe}_2\text{O}_4/g\text{-C}_3\text{N}_4$

The Sm- $\text{ZnFe}_2\text{O}_4/g\text{-C}_3\text{N}_4$  binary composite was synthesized by a simple co-precipitation method. First, 0.2g of Sm- $\text{ZnFe}_2\text{O}_4$  and 0.2g of  $g\text{-C}_3\text{N}_4$  were individually dissolved in 50 mL of water to obtain homogeneous solutions, which were then combined, stirred on stirrer for 15 minutes, and subsequently sonicated for 15 minutes to form a well-dispersed suspension. Then  $g\text{-C}_3\text{N}_4$  solution was added dropwise in Sm- $\text{ZnFe}_2\text{O}_4$  solution with burette and stirred for 30 minutes at room temperature. The resulting solution was sonicated for 15 minutes. This mixture was then heated in an electric oven, collected by centrifugation, and dried at 70°C in an oven. The conclusion by-product was crushed into fine nanoparticles using a mortar, and the resulting nanopowder was then burned at 500 °C within furnace for 3 hours, and collected in brown color shown in Figure 1 made in canva. By changing the  $g\text{-C}_3\text{N}_4$  content to be 20, 30 and 40 mg, the samples were named as SZF/GCN-X (X = 20, 30 and 40 mg) and their properties were analyzed by different characterization (Karthik et al., 2017).

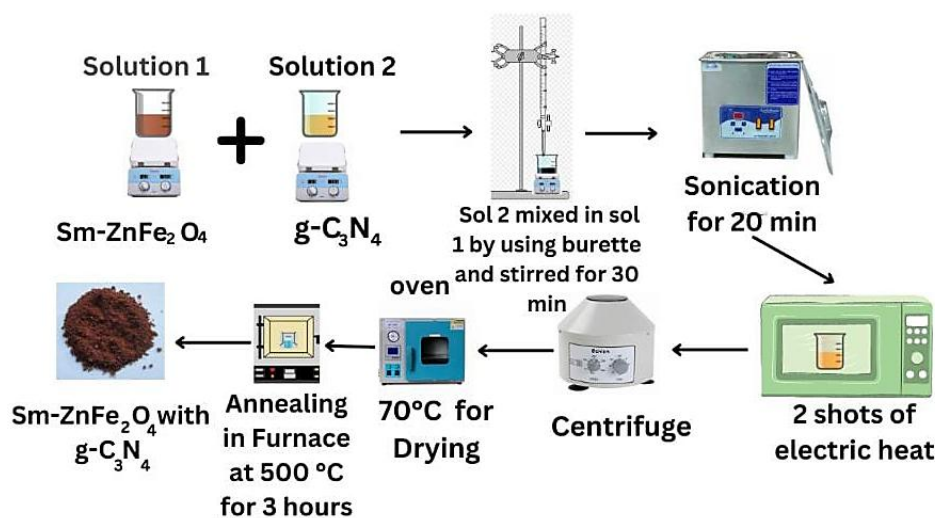


Fig. 1: illustration of the synthesis of Sm-  $\text{ZnFe}_2\text{O}_4/g\text{-C}_3\text{N}_4$

### Activity of Photocatalytic

For the purpose of evaluating the activity of photocatalytic, 50 ml of the RhB solution was added to a 250 mL beaker flask and it was mixed at 180 rpm. To find the equilibrium of desorption and adsorption between the photocatalyst and dye solution, 20 mg/50 ml and 30 mg/50 ml were distributed in the 50 ml RhB solution and exposed to darkness for 30 minutes. After 30 minutes in the dark, an oxidant

(H<sub>2</sub>O<sub>2</sub>) solution was added. After that the whole setup was exposed in sunlight. By using a LUX meter, the intensity of sunlight which was 1080 Wm<sup>2</sup> was measured. After centrifuging for 15 minutes the solution of 5mL volume was taken out from beakers and using of UV-Vis spectroscopy absorbance was determined (Sudha & Sivakumar, 2015). The efficiency was determined by using the following Eq. (1) (Jouyandeh et al., 2021):

$$\text{Photocatalytic efficiency } (\eta) = (1 - \frac{C_t}{C_0}) \times 100 \quad 1)$$

The dye concentration is indicating by C<sub>t</sub> after time 't.' C<sub>0</sub> indicate the dye's initial concentration, and 't' indicate for time.

#### Characterization

The structural features of ZnFe<sub>2</sub>O<sub>4</sub> and ZnFe<sub>2</sub>O<sub>4</sub> samples doped with Sm were analyzed through X-Ray Diffraction employing CuKα (λ = 1.54056 Å). The scanning angle ranged 20° to 80° (2θ), and the scanning rate was set at 2°/min. The structure of the creating samples was examined using a scanning electron microscope to analyze their morphology. The absorption bands were identified and checked using a FTIR spectrometer. Optical measurements in the wavelength (λ) range of 200-800 nm were conducted using a UV-Visible spectrometer (Singh et al., 2020).

### Results and Discussion

#### XRD Analysis

XRD analysis was used to estimate the phase and fundamenta information of synthesized Sm doped ZnFe<sub>2</sub>O<sub>4</sub> with g-C<sub>3</sub>N<sub>4</sub> nanocomposites. XRD widely used method to investigate structural properties as well as crystal solid sample's lattice parameters in powder form. The XRD results were taken with CuKα radiations with a 1.54056 wavelength at room temperature and angles ranging from 20° to 80°. Fig. shows the pattern of XRD of Sm -doped ZnFe<sub>2</sub>O<sub>4</sub> with g-C<sub>3</sub>N<sub>4</sub> with different concentrations of g-C<sub>3</sub>N<sub>4</sub>. In XRD spectra the Diffraction peaks were seen at 2θ = 29.69°, 35.88°, 43.19°, 53.3°, 57.25°, 62.91° where were indexed to (220), (311), (400), (422), (511), (440) crystal planes of Sm doped ZnFe<sub>2</sub>O<sub>4</sub> with g-C<sub>3</sub>N<sub>4</sub> with the JCPDS card data 89-1012, which showed the cubic structure respectively shown in Figure 2. The Sm doped ZnFe<sub>2</sub>O<sub>4</sub> with g-C<sub>3</sub>N<sub>4</sub> structure was successfully obtained, as demonstrated by the strong interaction between g-C<sub>3</sub>N<sub>4</sub> and ZnFe<sub>2</sub>O<sub>4</sub>. As the mass percentage of g-C<sub>3</sub>N<sub>4</sub> increased, g-C<sub>3</sub>N<sub>4</sub> diffraction peaks gradually increased (Bai et al., 2018). Doping with Sm ions indicate in a decrease of the crystallite size. The large surface area will be enhanced by the reduction in size. The crystallite size was calculated 30 nm, 26 nm and 24 nm. The crystallite size of a Sm doped ZnFe<sub>2</sub>O<sub>4</sub> with g-C<sub>3</sub>N<sub>4</sub> composite was estimated using the Debye-Scherrer equation (Karthik et al., 2017).

$$D = \frac{k\lambda}{\beta \cos\theta} \quad 2)$$

The variables in this equation are the average size of crystallites (D), (FWHM) in radians (β), the angle of diffraction (θ), or Bragg's angle (measured from the 2θ scale), and a constant of proportionality called Scherer's constant that is shape-dependent and size distribution of the crystallite structure. In most cases, this constant is taken to be k = 0.9.

#### SEM-EDX Analysis

The SEM images show Sm<sup>3+</sup> morphology for zinc ferrite with g-C<sub>3</sub>N<sub>4</sub> having some agglomeration with uniform distribution of particles; nonmetal (samarium) doping in the zinc ferrite lattice resulted in The SEM images demonstrate Sm<sup>3+</sup> morphology for zinc ferrite with g-C<sub>3</sub>N<sub>4</sub> having some clustering with uniform particle distribution; nonmetal (samarium) doping in the zinc ferrite lattice led to enhanced particle aggregation, possibly because of a decrease in surface area caused by the formation of interstitial spaces from samarium doping and with varying amounts of g-C<sub>3</sub>N<sub>4</sub> enhanced aggregation of particles, which may be owing to an reduced in surface area as a result of formation of interstitial spaces due to doping of samarium and with different amount of g-C<sub>3</sub>N<sub>4</sub>. The average grain size of manufactured SZG1, SZG2, SZG3 nanocomposites was stimate to be 0.08 nm, 0.13 nm, 24.15 nm, as demonstrated by using Image j software. Using energy-dispersive spectroscopy, the element contained in the prepared Sm<sup>3+</sup> doped ZnFe<sub>2</sub>O<sub>4</sub> with g-C<sub>3</sub>N<sub>4</sub> was examined. Zn, Fe, and O elements show that the composite was prepared. Certain impurities in the sample are revealed by a small amount of other elements (Karthik et al., 2017; Kannan et al., 2020).

#### FT-IR Analysis

For identifying functional groups in prepared nanomaterials FTIR is the most effective and dynamic method available. FTIR can be used to determine the bonding that is present in the material. The FTIR characteristic peaks of Samarium-doped zinc ferrite with g-C<sub>3</sub>N<sub>4</sub> in the range of 400-5000 cm<sup>-1</sup> (Yang et al., 2014). The Fe-O and Zn-O vibrations in the Sm- ZnFe<sub>2</sub>O<sub>4</sub> appear in the 400-600 cm<sup>-1</sup> range, confirming the ferrite structure, with potential peak shifts because of Sm doping. The triazine ring appears around 812 cm<sup>-1</sup> for the g-C<sub>3</sub>N<sub>4</sub> component, while C-N and C=N stretching vibrations are detected between 1200-1600 cm<sup>-1</sup>. Chemical bonding can be indicated by shifts in the C=N or Fe-O peaks caused by interactions between the two components.

#### 4.5.2 UV-Visible Spectroscopy Analysis

The optical properties of semiconducting nanomaterials are investigated using UV-visible spectra. The optical bandgap (E<sub>g</sub>) of a material can be computed using a Tauc plot. The band gap, absorption spectrum, and absorption edge for the synthesized Sm doped ZnFe<sub>2</sub>O<sub>4</sub> with g-C<sub>3</sub>N<sub>4</sub> (Manohar et al., 2021). It can be seen that the The absorption peak typically shifts towards a longer wavelength as the g-C<sub>3</sub>N<sub>4</sub> concentration in the Sm doped ZnFe<sub>2</sub>O<sub>4</sub> increase. The equation mentioned as was utilized to determine the optical band gap (Wang et al., 2019).

$$chv = A (hv - E_g)^n \quad 3)$$

The ( $\alpha$ ) absorption coefficient is estimated in  $\text{cm}^{-1}$ , while characteristic parameter represents ( $A$ ). Planck's constant denotes ( $h$ ), show frequency ( $\nu$ ), optical band gap energy represents ( $E_g$ ) and  $A$  variable unique to the transition process is ( $n$ ). The respective band gap values at different contents of  $g\text{-C}_3\text{N}_4$  nanocomposites are determined as 1.41 eV, 1.32 eV and 1.24 eV respectively. It confirms that the hybrid ferrites nano-composite has superior visible light absorption capacity.

#### 4.3 Dielectric Properties

Determining how the dielectric parameters of nanocomposites, specifically the tangent loss ( $\tan \delta$ ) and dielectric constant ( $\epsilon'$ ), affect their electrical properties. The tangent loss evaluates the amount of energy lost as heat throughout an electric field's cycle, whereas the dielectric constant shows a material's ability to hold electric field-containing electrical energy. These parameters are play a vital role in the field of nanocomposites (Koops, 1951). The increased capacity of nanocomposites with a higher dielectric constant to store electrical energy makes them advantageous for energy storage devices like capacitors. On the other hand, tangent loss values represent the amount of energy dissipated as well as the possibility of effective dielectric properties of heating. Increased  $\tan \delta$  values indicate potential uses in fields such as microwave heating and flexible electronics development.

The ability of the material to retain electric polarization is indicated by the real part of dielectric permittivity ( $\epsilon'$ ), whereas the imaginary part ( $\epsilon''$ ) indicates its ability to dissipate power through electric loss. The formula is used to calculate  $\epsilon$  (Ansari et al., 2018):

$$\epsilon' = \frac{ct}{A\epsilon_0} \quad 4)$$

Here, "c" and "t" indicates for the samples' capacitance and thickness, respectively, and "A" indicate for the pellet's surface area and the permittivity of free space, which has a value of  $8.85 \times 10^{-12} \text{ m}^{-3} \text{ kg}^{-1} \text{ s}^4 \text{ A}^2$ . The loss factor of a dielectric material,  $\epsilon''$ , is calculated by the equation: (Muhammad & Iqbal, 2016)

$$\epsilon'' = \tan \delta \times \epsilon' \quad 5)$$

Here,  $\epsilon''$  denotes the loss factor, while  $\delta$  indicate the loss angle. The dielectric constant ( $\epsilon'$ ) throughout all samples varies with applied frequency, Compared to the substituted samples, the pure sample ( $x = 0.0$ ) notably shows a lower frequencies and a lower dielectric constant. Impact of various parameters on the degradation of RhB

#### Effect of pH

The ability of the photocatalyst to degrade RhB under sunlight is depends upon the pH level of the solution. The research was conducted to examine the impact of pH on the degradation of RhB. For this purpose at various pH ranges 2-10 the ability of the photocatalyst degradation of RhB checked. Diluted HCl or NaOH was used to change the pH of the solution. The highest photo degradation of RhB using of Sm doped  $\text{ZnFe}_2\text{O}_4$  with  $g\text{-C}_3\text{N}_4$  at different concentrations were attained at pH 9 and 8. It was found that more degradation was seen at a particular dye solution pH. Using of Sm doped  $\text{ZnFe}_2\text{O}_4$  with  $g\text{-C}_3\text{N}_4$  at different concentration composites the effectiveness of degradation of RHB was 98.3% at pH 8 in 70 minutes. At this pH, positive holes are important oxidising species, and the nanocomposite also functions as a photosensitizer. Hydroxyl radicals (OH) can be produced by the photogenerated hole in the valence band of the nanocomposite due to its sufficient positive redox potential (Pattnaik et al., 2018).

#### Effect of Catalyst Concentration

The photocatalyst's quantity in the dye solution determines how effective it is for the degradation process. As the dosage of the catalyst was enhanced from 10 to 80 mg for 50ml dye solution at pH 8 and irradiated for 70 min, the percentage degradation of the Rh B dye was analyzed to enhance for all the catalysts. Maximum degradation of Sm doped  $\text{ZnFe}_2\text{O}_4$  with  $g\text{-C}_3\text{N}_4$  at different concentration was observed at 60 mg was enhanced from 72 to 98.3%. Increased active sites on the catalyst's surface are considered to be the cause of the increased degradation because they increase the formation of hydroxyl radicals, which further accelerates the degradation process. Additionally, it was noted that a continued rise in photocatalst dosage led to a decrease in degradation efficiency in all samples (Abdellah et al., 2018). The cause of this is that as the catalyst dose increases, the number of active sites enhanced so penetration of light slow due to shielding effect.

#### Effect of $\text{H}_2\text{O}_2$ Dose

Oxidants ( $\text{H}_2\text{O}_2$ ) are essential in photo-degradation as they prevent the recombination of ( $e^- - h^+$ ) pairs by capturing electrons. When a catalyst and an oxidant ( $\text{H}_2\text{O}_2$ ) are present, Rhodamine B dye undergoes complete oxidation. To optimize the oxidant dose, the concentration of  $\text{H}_2\text{O}_2$  was varied from 2 to 14 mM. The graph indicates that increasing the oxidant dose causes degradation to increase, but only to a certain point, after which it begins to decrease (Soleimani & Rahmani, 2022). In order to optimise  $\text{H}_2\text{O}_2$ , the following experimental parameters were used: pH = 8 = 60 mg for Sm doped  $\text{ZnFe}_2\text{O}_4$  with  $g\text{-C}_3\text{N}_4$  at different concentration 10 ppm RhB dye concentration, and 70min irradiation time maximum degradation occurs which is 98.3%. The effects of varying  $\text{H}_2\text{O}_2$  concentrations from 2 to 14 mM on RhB photo degradation (Kumar et al., 2009)

#### Effect of Irradiation Time

The effect of irradiation time on removal (%) at optimum conditions was analyzed and represented. In the early stages of irradiation, a pronounced rise was noted in the RhB degradation. With time, the rate of degradation slows down. The catalyst's active site needs a certain amount of time to completely degrade RhB. This is because OH radicals are produced influenced by the solution's pH, the degradation rate in removal processes gradually slows down. The catalyst's active site is inhibited by the reaction of hydroxyl ions with ferrous, which suppresses the Fenton-like reaction (Singh et al., 2020).

## Reusability

It is vital to look into a photocatalyst's stability and reusability from an environmental and economic point of view. When the completion of the degradation reaction, the magnet was used to restore the composites, which were then cleaned three times in distilled water and oven-dried at 80 °C before being used again for a later cycle. Every composite undergoes a reusability study under the same ideal circumstances, i.e., pH 8, oxidant dose 10 mM, composite dosage 60 mg/50 mL for different concentration of Sm doped ZnFe<sub>2</sub>O<sub>4</sub> with g-C<sub>3</sub>N<sub>4</sub>. With little loss in product yield, the photocatalyst can be reused up to five times while maintaining 85% photocatalytic activity (Kannan et al., 2020).

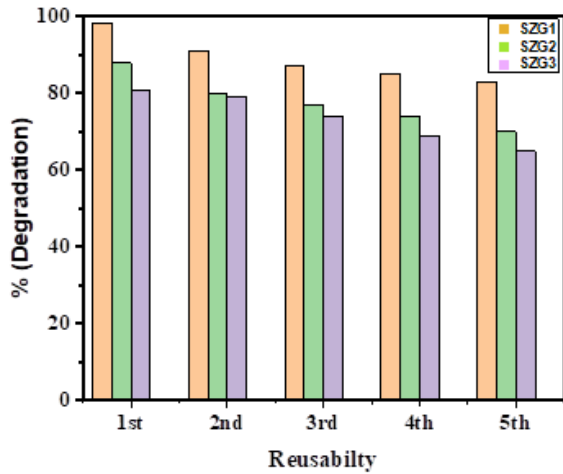
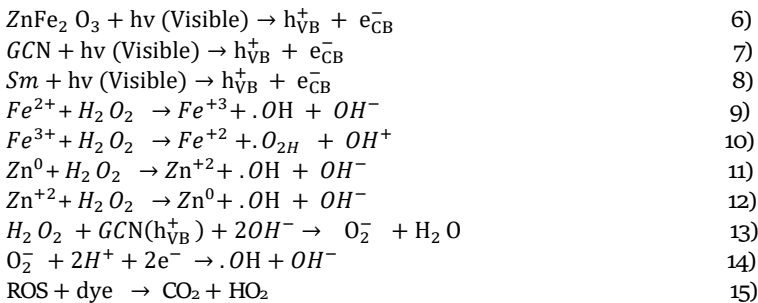


Fig. 2: Effects of Sm-ZnFe<sub>2</sub>O<sub>4</sub>/g-C<sub>3</sub>N<sub>4</sub>-X (X=0.2, 0.3, 0.4) Reusability on degradation efficiency



## Photodegradation Mechanism

A photocatalytic mechanism is illustrated in Figure 3. Both Sm-ZnFe<sub>2</sub>O<sub>4</sub> and g-C<sub>3</sub>N<sub>4</sub> can be excited and generate light-induced e<sup>-</sup> and h<sup>+</sup> when exposed to visible light. The Sm-ZnFe<sub>2</sub>O<sub>4</sub> valence band (VB) readily absorbs photo induced e<sup>-</sup> in the g-C<sub>3</sub>N<sub>4</sub> conduction band (CB). Consequently the O<sub>2</sub> anion reacts with H<sub>2</sub>O<sub>2</sub> to generate the hydroxyl radical, which efficiently degrade the RhB dye. RhB degrades into CO<sub>2</sub>, H<sub>2</sub>O. Hence, it proposes the Sm doped ZnFe<sub>2</sub>O<sub>4</sub> with g-C<sub>3</sub>N<sub>4</sub> composite as a photocatalyst, possessing effective photocatalytic activity, prolonged charge carrier lifetime, and increased charge separation efficiency (Raza et al., 2020). Specifically, Sm can encourage the flow of electrons from ZnFe<sub>2</sub>O<sub>4</sub> to g-C<sub>3</sub>N<sub>4</sub> and suppress movement in reverse of electrons to ZnFe<sub>2</sub>O<sub>4</sub>. Consequently, photoactivity of Sm doped ZnFe<sub>2</sub>O<sub>4</sub> with g-C<sub>3</sub>N<sub>4</sub> was significantly improved. Some steps are involved in this process from eq (6-15) (Fatima, et al., 2024). In photocatalysis, materials absorb photons denoted as hν, where h is Planck's constant and ν is the frequency of light with energy equal to or greater than their bandgap. This absorption excites electrons from the valence band to the conduction band, generating electron-hole pairs. These pairs can migrate to the material's surface, where they participate in oxidation and reduction reactions, leading to the degradation of pollutants or other chemical transformations.

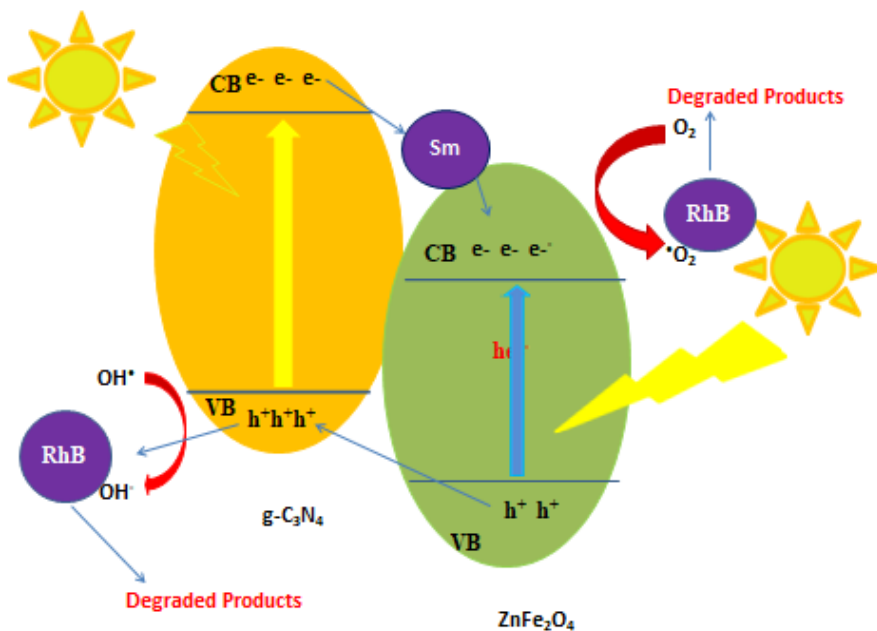


Fig. 3: Schematic diagram of photocatalytic activity

## Conclusion

This study introduces the novel application of Sm doped ZnFe<sub>2</sub>O<sub>4</sub> supported by g-C<sub>3</sub>N<sub>4</sub> as an electron mediator for the first time. Sm doped ZnFe<sub>2</sub>O<sub>4</sub> with g-C<sub>3</sub>N<sub>4</sub> was found to be an effective photocatalyst. For the environmental degradation of dyes in solar light irradiation Sm doped ZnFe<sub>2</sub>O<sub>4</sub> with g-C<sub>3</sub>N<sub>4</sub> composite was fabricated successfully using a simple co-Precipitation strategy and was clearly defined by comprehensive analyses using UV-Vis spectroscopy, SEM-EDX, XRD, DIELECTRIC and FTIR techniques. Sm doped ZnFe<sub>2</sub>O<sub>4</sub> with g-C<sub>3</sub>N<sub>4</sub> (SZG3) composite exhibited 98.3% improved photodegradation of RhB in 70 min at ideal conditions such as pH (8), composite dosage (60 mg/50 mL) and H<sub>2</sub>O<sub>2</sub> dosage (10 mM). Compared to SZG1, SZG2, the SZG3 composite demonstrated enhanced photocatalytic activity. Key attributes of the Sm doped ZnFe<sub>2</sub>O<sub>4</sub> with g-C<sub>3</sub>N<sub>4</sub> composite include its straightforward synthesis process, excellent photocatalytic capabilities, magnetic recoverability, and notable durability. This work proposes a novel approach to improving the photo efficiency and recyclability of g-C<sub>3</sub>N<sub>4</sub> based photocatalysts through the Sm doped ZnFe<sub>2</sub>O<sub>4</sub> with g-C<sub>3</sub>N<sub>4</sub> composite.

## References

- Ansari, M. A. H., Jha, A. K., Akhter, Z., & Akhtar, M. J. (2018). Multi-band RF planar sensor using complementary split ring resonator for testing of dielectric materials. *IEEE Sensors Journal*, 18(16), 6596-6606. <https://doi.org/10.1109/JSEN.2018.2822877>.
- Abdellah, M. H., Nosier, S. A., El-Shazly, A. H., & Mubarak, A. A. (2018). Photocatalytic decolorization of methylene blue using TiO<sub>2</sub>/UV system enhanced by air sparging. *Alexandria Engineering Journal*, 57(4), 3727-3735. <https://doi.org/10.1016/j.aej.2018.07.018>.
- Abdulhamid, M. A., & Muzamil, K. (2023). Recent progress on electrospun nanofibrous polymer membranes for water and air purification: A review. *Chemosphere*, 310, 136886. <https://doi.org/10.1016/j.chemosphere.2022.136886>.
- Bai, S., Zhang, N., Gao, C., & Xiong, Y. (2018). Defect engineering in photocatalytic materials. *Nano Energy* 53(1), 296-336. <https://doi.org/10.1016/j.nanoen.2018.08.058>.
- Bera, S., Ghosh, S., & Basu, R. N. (2018). Fabrication of Bi<sub>2</sub>S<sub>3</sub>/ZnO heterostructures: An excellent photocatalyst for visible-light-driven hydrogen generation and photoelectrochemical properties. *New Journal of Chemistry*, 42(1), 541-554. <https://doi.org/10.1039/C7NJ03424E>.
- Ebrahimi, M., Rasouliyan, M., Panahiyan, H., & Ghodrati, H. (2021). Designing the evaluation model for sustainable technology in the textile industry. *Journal of System Management* 7(3), 143-161. <https://doi.org/10.30495/jsm.2021.1938796.1513>.
- Fu, J., Yu, J., Jiang, C., & Cheng, B. (2018). g-C<sub>3</sub>N<sub>4</sub>-Based heterostructured photocatalysts. *Advanced Energy Materials*, 8(3), 1701489-1701503. <https://doi.org/10.1002/aenm.201701503>.
- Faheem, M., Siddiqi, H. M., Habib, A., Shahid, M., & Afzal, A. (2022). ZnO/Zn (OH)<sub>2</sub> nanoparticles and self-cleaning coatings for the photocatalytic degradation of organic pollutants. *Frontiers in Environmental Science*, 10(2), 965912-965925. <https://doi.org/10.3389/fenvs.2022.965925>.
- Fatima, A., Nadeem, N., Saleh, B., Rehan, Z. A., Noreen, S., Ali, H. T., & Zahid, M. (2024). Harnessing the sunlight to degrade dye using polythiophene-based silver doped ZnS composite. *Chalcogenide Letters*, 21(11), 895-915. <https://doi.org/10.15251/CL.2024.2111.895>.
- Jouyandeh, M., Khadem, S. S. M., Habibzadeh, S., Esmaili, A., Abida, O., Vatanpour, V., & Varma, R. S. (2021). Quantum dots for photocatalysis: synthesis and environmental applications. *Green Chemistry*, 23(14) 4931-4954. <https://doi.org/10.1039/D1GC00639H>.
- Muhammad, R., & Iqbal, Y. (2016). Enhanced dielectric properties in Nb-doped BT-BMT ceramics. *Ceramics International*, 42(16), 19413-19419. <https://doi.org/10.1016/j.ceramint.2016.08.152>.
- Koops, C. G. (1951). On the dispersion of resistivity and dielectric constant of some semiconductors at audiofrequencies. *Physical Review*, 83(1), 121.
- Kumar, P. S. S., Raj, M. R., Anandan, S., Zhou, M., & Ashokkumar, M. (2009). Visible light assisted photocatalytic degradation of acid red 88 using Au-ZnO nanophotocatalysts. *Water Science and Technology*, 60(6) 1589-1596. <https://doi.org/10.2166/wst.2009.496>.
- Karthik, K., Dhanuskodi, S., Gobinath, C., Prabukumar, S., & Sivaramkrishnan, S. (2017). Photocatalytic and antibacterial activities of hydrothermally prepared CdO nanoparticles. *Journal of Materials Science: Materials in Electronics*, 28(1) 11420-11429. <https://doi.org/10.1007/s10854-017-6937-z>.
- Kannan, S., Subiramaniam, N. P., & Sathishkumar, M. (2020). A novel green synthesis approach for improved photocatalytic activity and antibacterial properties of zinc sulfide nanoparticles using plant extract of *Acalypha indica* and *Tridax procumbens*. *Journal of Materials Science: Materials in Electronics*, 31(12) 9846-9859. <https://doi.org/10.1007/s10854-020-03529-x>.
- Mousavi, S. M., Pouramini, Z., Babapoor, A., Binazadeh, M., Rahmani, V., Gholami, A., & Rahman, M. M. (2024). Photocatalysis air purification systems for coronavirus removal: Current technologies and future trends. *Chemosphere*, 12(1) 141525-141534. <https://doi.org/10.1016/j.chemosphere.2024.141525>.
- Mamba, G., & Mishra, A. K. (2016). Graphitic carbon nitride (g-C<sub>3</sub>N<sub>4</sub>) nanocomposites: a new and exciting generation of visible light driven photocatalysts for environmental pollution remediation. *Applied Catalysis B: Environmental*, 19(8) 347-377. <https://doi.org/10.1016/j.apcatb.2016.05.052>.
- Manohar, A., Park, J., Geleta, D. D., Krishnamoorthi, C., Thangam, R., Kang, H., & Lee, J. (2021). Synthesis and characterization of ZnO nanoparticles for photocatalysis, antibacterial and cytotoxicity in kidney cancer (A498) cell lines. *Journal of Alloys and Compounds*, 874(2) -159851-159868. <https://doi.org/10.1016/j.jallcom.2021.159868>.
- Pattnaik, S. P., Behera, A., Martha, S., Acharya, R., & Parida, K. (2018). Synthesis, photoelectrochemical properties and solar light-induced photocatalytic activity of bismuth ferrite nanoparticles. *Journal of Nanoparticle Research*, 20(2) 1-15. <https://doi.org/10.1007/s11051-017-4110-5>.
- Rawal, S. B., Bera, S., Lee, D., Jang, D. J., & Lee, W. I. (2013). Design of visible-light photocatalysts by coupling of narrow bandgap semiconductors and TiO<sub>2</sub>: effect of their relative energy band positions on the photocatalytic efficiency. *Catalysis Science &*

- Technology*, 3(7) 1822-1830, <https://doi.org/10.1039/C7NJ03424>.
- Rabiee, N., Ahmadi, S., Afshari, R., Khalaji, S., Rabiee, M., Bagherzadeh, M., & Webster, T. J. (2021). Polymeric nanoparticles for nasal drug delivery to the brain: relevance to Alzheimer's disease. *Advanced Therapeutics*, 4(3) 12-76, <https://doi.org/10.1002/adtp.202000076>.
- Raza, N., Raza, W., Gul, H., Azam, M., Lee, J., Vikrant, K., & Kim, K. H. (2020). Solar-light-active silver phosphate/titanium dioxide/silica heterostructures for photocatalytic removal of organic dye. *Journal of Cleaner Production*, 254(2) 120031-120054, <https://doi.org/10.1016/j.jclepro.2020.120031>.
- Sudha, D., & Sivakumar, P. (2015). Review on the photocatalytic activity of various composite catalysts. *Chemical Engineering and Processing: Process Intensification*, 97(2) 112-133, <https://doi.org/10.1016/j.cep.2015.08.006>.
- Singh, J., & Dhaliwal, A. S. (2020). Plasmon-induced photocatalytic degradation of methylene blue dye using biosynthesized silver nanoparticles as photocatalyst. *Environmental Technology*, 41(12), 1520-1534. <https://doi.org/10.1080/09593330.2018.1540663>.
- Soleimani, F., & Rahmani, M. B. (2022). Investigating the structural, optical, and photocatalytic activity of TiO<sub>2</sub>/SnO<sub>2</sub> nanocomposites synthesized by the facile sol-gel technique for dye degradation. *Physica Scripta*, 97(12), 125811-125822, <https://doi.org/10.1088/1402-4896/aca057>.
- Shahraki, H. S., Bushra, R., Shakeel, N., Ahmad, A., Ahmad, M., & Ritzoulis, C. (2023). Papaya peel waste carbon dots/reduced graphene oxide nanocomposite: from photocatalytic decomposition of methylene blue to antimicrobial activity. *Journal of Bioresources and Bioproducts*, 8(2), 162-175, <https://doi.org/10.1016/j.jobab.2023.01.009>.
- Ullah, R. (2023). Semiconductor ZnFe<sub>2</sub>O<sub>4</sub> as efficient photocatalyst for the degradation of organic dyes: an update. *Journal of Chemical Reviews*, 5(4) 466-476, <https://doi.org/10.2166/wst.2009.496>.
- Wang, M., He, L., Wang, M., Chen, L., Yao, S., Jiang, W., & Chen, Y. (2019). Simultaneous removal of NH<sub>3</sub>-N and COD from shale gas distillate via an integration of adsorption and photo-catalysis: A hybrid approach. *Journal of Environmental Management*, 249, 109342. <https://doi.org/10.1016/j.jenvman.2019.109342>
- Yang, Y., Guo, W., Guo, Y., Zhao, Y., Yuan, X., & Guo, Y. (2014). Fabrication of Z-scheme plasmonic photocatalyst Ag@ AgBr/g-C<sub>3</sub>N<sub>4</sub> with enhanced visible-light photocatalytic activity. *Journal of Hazardous Materials*, 271(20), 150-159, <https://doi.org/10.1016/j.jhazmat.2014.02.023>.